Structural and Thermodynamic Properties of Pb-Cd-Te Thin Films: Experimental Study and DFT Analysis

B. Naidych, T. Parashchuk, I. Yaremiy, M. Moyseyenko, O. Kostyuk, O. Voznyak, Z. Dashevsky & L. Nykyruy

Journal of Electronic Materials

ISSN 0361-5235

Journal of Elec Materi
DOI 10.1007/s11664-020-08561-5

Springer

Journal of ELECTRONIC MATERIALS
https://doi.org/10.1007/s11664-020-08561-5

Structural and Thermodynamic Properties of Pb-Cd-Te Thin Films: Experimental Study and DFT Analysis

B. NAIDYCH,[1,5] T. PARASHCHUK,[1,4] I. YAREMIY,[1] M. MOYSEYENKO,[2] O. KOSTYUK,[1,2] O. VOZNYAK,[1] Z. DASHEVSKY,[3] and L. NYKYRUY[1]

1.—Vasyl Stefanyk Precarpathian National University, Shevchenko Str. 57, Ivano-Frankivsk 76018, Ukraine. 2.—Ivano-Frankivsk National Medical University, Halytska Str. 2, Ivano-Frankivsk 76000, Ukraine. 3.—Ben-Gurion University of the Negev, 84105 Beer-Sheva, Israel. 4.—Present address: The Lukasiewicz Research Network – Krakow Institute of Technology, Zakopianska Str. 73, 30-418 Kraków, Poland. 5.—e-mail: bvolochanska@i.ua

Vacuum evaporation technology was applied to fabricate $Pb_{0.9}Cd_{0.1}Te$:Pb (3 at.%) thin films on glass and polycrystalline silicon substrates. X-ray diffraction analysis confirms the rock salt structure with the (100) preferred growing direction for the investigated films. The formation of films on an amorphous glass substrate occurs by two consecutive growth mechanisms. The Volmer–Weber mechanism is the initial mechanism, and it gradually changes with the Frank–van der Merve mechanism. On the polycrystalline silicon substrate, the Volmer–Weber growth mechanism is dominant. Surface formations are oriented and needle-like. A complex of thermodynamic parameters: the enthalpy of formation, entropy, Gibbs free energy, and heat capacity were calculated using the estimated crystallographic data. This work brings light on the fabrication process of single-phase $Pb_{0.9}Cd_{0.1}Te$:Pb (3 at.%) thin films with a high-quality surface using the low-cost and simple vacuum evaporation method.

Key words: Thin films, thermodynamic properties, ab initio calculations, XRD analysis, solid solution

INTRODUCTION

Pb-Cd-Te solid solution is a promising material for the fabrication of thermoelectric modules over a medium temperature range.[1] Due to the isoelectronic effect of cadmium (Cd) atoms in lead telluride (PbTe), this material can be used for the fabrication of both *n*- and *p*-type thermoelectric legs.[2] Thin films based on Pb-Cd-Te are extremely interesting for application in miniature devices or various flexible systems, such as thermoelectric micromodules.[3,4] The microstructure has a decisive influence on the properties of thin films.[5] On the other hand, deposition and heat treatment technologies are reliable for achieving suitable and stable characteristics. If the dimensionless figure of merit for bulk materials is sufficiently high, this parameter for thin films is still a challenge.[5–8]

The solubility limit of Cd in the PbTe matrix can be up to 15%.[9,10] The formation of such a solid solution is atypical because of the significant difference of its components in the crystal structures (sphalerite for CdTe and rock-salt-type for PbTe) and the bandgaps [E_g (CdTe) = 1.534 eV[11] and E_g (PbTe) = 0.31 eV[12]]. On the other hand, the formation of the single-phase solid solution is energetically advantageous due to the proximity of lattice constants. PbTe and CdTe crystallize in a cubic modification with similar values of the lattice constants: 6.4611 Å[13] and 6.4820 Å, respectively.[14] Excessive doping by bivalent elements (including cadmium) leads to the derivation of nanoscale precipitations which are effective scattering centers for phonon propagation.[15]

(Received April 26, 2020; accepted October 10, 2020)

Published online: 11 November 2020

Lead telluride-based solid solutions crystallize in a rock-salt structure.[6] According to density functional theory (DFT) calculations,[9,10] the energy of such material in a cubic rock-salt lattice structure is lower than if the same composition is formed by a sphalerite crystal lattice. In the case of lead-cadmium-telluride, cadmium atoms substitute lead (Pb).[16] The electroneutral cadmium atom substitution in the lead position is a dominant point defect.[2] On the other hand, the behavior of the neighboring atoms and modification of the structure due to the presence of a Cd atom remains unclear.

Modeling of the crystal structure of such material is especially important in the case of thin films. The film morphology is related to the stability of its surface. Crystal structures tend to minimize their total surface energy, according to Woolf's theorem. First, the surface contains discontinuities of the periodic crystalline potential and defects of the base crystal. Incomplete bonds are partially rearranged, for example, forming dimers, surface reconstructions, or remaining as broken bonds. Atoms on the surface can be repositioned vertically or sideways, forming new bonds and resulting in surface reconstruction.[17–19] The surface energy depends on the orientation of the crystal and the reconstruction of the surface, i.e. the possible permutation of the surface bonds and atoms.[17,18] The reduction of the number of broken bonds on the surface decreases its energy, while the distortion of the bonds increases such energy.

Another important factor for the formation of the surface of films is the structure of the substrate. Discrepancies in the values of the lattice parameter of the film and substrate material cause internal stresses at the boundary of these materials.[20,21] Accordingly, changing the substrate material and temperature growth modes can affect the structure of the film, the shape and size of the surface formations, and its properties for applications. Such film growth is described in some other studies. For example, in[22] the epitaxial growth of polycrystalline PbTe films on Si and glass substrates was observed. Thus, according to[23] the epitaxy occurs when the crystal structure of the film and the substrate are similar, as we have observed for the lattice constant of PbTe and CdTe.

In this work, we investigate the crystal structure modification for $Pb_{1-x}Cd_xTe$ thin films due to the presence of Cd. The thermodynamic properties of Pb-Cd-Te films have been calculated using the first-principle method and rigid band approximation. Such analysis clarifies the crystal reorganization during film growth. Furthermore, using the low-cost and simple vacuum evaporation method, the fabrication of single-phase $Pb_{0.9}Cd_{0.1}Te$:Pb (3 at.%) films with a high-quality surface was carried out, making this a promising material for application in film thermoelectric modules.

EXPERIMENTAL AND COMPUTATIONAL DETAILS

Pre-synthesized $Pb_{0.9}Cd_{0.1}Te$:Pb (3 at.%) material was used for film fabrication. Synthesis of the compound was carried out by the melting of components in sealed quartz ampoules evacuated to a residual pressure of 0.01 Pa. The ampoules were subjected to rigorous purification, which included washing in $1HNO_3$:3HCl concentrated acid mixture and frequent cleaning with distilled water and isopropanol. Only highly pure initial components Pb (99.999), Cd (99.999), and Te (99.999) were used for the synthesis.

Pb-Cd-Te thin films were deposited by open vacuum evaporation technology on glass and polycrystalline silicon (Si) substrates. The temperature of the substrate and evaporator was T_S = 473 K and T_E = 833 K, respectively. The thicknesses of the films were determined by the time of deposition in the range of 20–80 s. The scanning electron microscopy analyses were performed using a JEOL JSM-6460LV scanning electron microscope.

The structure of the deposited films was examined with an X-ray diffractometer using $Cu_{K\alpha}$ radiation. X-ray diffractometry results were processed by the Rietveld method using FullProf.2k (version 5.30) from the WinPLOTR software package. The details of the use of these techniques are described in Ref. 24. The possible prevailing orientation (texture) of the main phase grains was determined using the Marsh–Dollas prevailing orientation.[25]

A thermodynamic method, based on minimizing the total energy of the cluster, was used to study the energy characteristics. The estimation of the local minimum on the potential energy surface and the calculation of the energies of vibrational spectra were performed using GAMESS quantum-chemical software.[26,27] The spin-restricted Hartree–Fock (RHF) method and the hybridized basis set B3LYP[25,28] with the Stevens–Basch–Krauss–Jasien–Cundari (SBKJC) parameterization were used. The high accuracy of this approach for both structural and thermodynamic properties of solids has been confirmed in many papers (see, e.g.[9,29]). The elastic properties of ideal PbTe crystals were determined using the method, based on the stress–strain relationship, described in Refs. 30, 31.

The enthalpy of formation H of a crystal can be determined using the rigid molecule approximation[32] from the following expression:

$$H \approx H_{\text{elec}} + H^0_{\text{vib}} + E_{\text{vib}}(T) + H_{\text{rot}}(T) + H_{\text{trans}}(T) + RT, \quad (1)$$

where H_{elec} is the electronic component of enthalpy, H_{vib} is the vibrational component of enthalpy, H^0_{vib} is the enthalpy of the zero-point vibration, H_{rot} is the rotational component of enthalpy, H_{trans} is the

translational component of enthalpy, R is the universal gas constant, and T is the temperature. A similar approach was used for the calculations of formation energy ΔE for the crystal.

The entropy of the crystal is the sum of the components:

$$\Delta S = S_{\text{trans}} + S_{\text{rot}} + S_{\text{vib}} + S_{\text{elec}} - nR[\ln(nN_0) - 1], \quad (2)$$

where N_0 is the Avogadro constant, n is the number of moles of molecules, and M is the mass of the molecule.

After calculating the contributions of entropy and enthalpy, the Gibbs energy of the crystal at a given temperature T can be calculated as follows:

$$\Delta G = H_{\text{elec}} + H^0_{\text{vib}} + H_{\text{vib}}(T) + H_{\text{rot}}(T) + H_{\text{trans}}(T) + RT - T(S_{\text{trans}} + S_{\text{rot}} + S_{\text{vib}} + S_{\text{elec}} - nR[\ln(nN_0 - 1]). \quad (3)$$

The calculations of the specific heat capacity were derived using the above thermodynamic potentials.

The construction of the clusters used for the calculations was studied in detail in previous works[33–35] for binary compounds. In our case, structural modeling was performed regarding the results of the defect subsystem analysis. The computer simulation of the surface effect on the thermodynamic parameters has been studied for lead selenide films.[36] For solid solutions with a small quantity of Cd atoms, the possible defect states should be considered, as shown in previous works.[9,37,38]

RESULTS AND DISCUSSION

The developed small cluster models have been used for a study of the film surface. Consequently, the determining factors affecting the physical properties are the structure of the surface layers. In this case, the influence of three-, four-, and five-coordinated atoms (surface atoms) becomes more determinative on the finite parameters than the atoms in the bulk (six-coordinated atoms). On the other hand, the agreement with the experimental data for the case of small clusters indicates sufficient accuracy of the proposed method.

The properties of $Pb_{1-x}Cd_xTe$ solid solutions were determined using the developed cluster models. These models consist of 8, 27, 56, and 64 atoms; each model corresponds to the rock-salt structure (Fig. 1). The first model of Pb_4Te_4 (Fig. 1a) consists of four atoms of lead and four atoms of tellurium. The second model of $Pb_{13}Cd_1Te_{13}$ (Fig. 1b) consists of 13 atoms of lead, 13 atoms of tellurium, and one cadmium. This model takes into account only the location of the Cd atom inside the cluster. The third ($Pb_{25}Cd_3Te_{28}$) (Fig. 1c) and fourth ($Pb_{29}Cd_3Te_{32}$) (Fig. 1d) models also consider the possibility of Cd location on the surface of the cluster, which is very important in the case of the thin films.

The main attention in the construction of cluster models was paid to the symmetry and the electric charge of the clusters to avoid distortion of the structure due to surface forces. The number of bonds of an atom with its neighbor determines the number of six-, five-, four-, and three-coordinated atoms in each model. This approach allows us to construct a system of equations for the estimation of the thermodynamic parameters of the clusters.

X-ray structural data analysis[39,40] indicates that the predominant growth directions of the thin films of PbTe-based materials are (100) and (110). The model images of such surfaces in the given crystallographic projections are shown in Fig. 2.

X-ray diffraction revealed that the structure of the sample remained a single phase within the detection limit of the instrument, and the positions of the atoms correspond to the structure of the rock salt. With the increase of cadmium content, the lattice parameter exhibits a linear tendency to decrease (Fig. 3).

The lattice parameter and energy structure of $Pb_{1-x}Cd_xTe$ crystals were calculated[9,10] using a tight-binding description of constituent materials and virtual crystal approximation. The obtained data shows that the rock-salt structure is more energy-efficient for Pb-Cd-Te solid solutions. Moreover, the introduction of cadmium atoms into the PbTe matrix changes the structure only after its content is more than 0.8 at.%. The atom of Pb began to disorient the neighboring atoms in the CdTe matrix already at the content of $\sim$ 0.25 at.%

According to the X-ray structural analysis, the predominant (200) direction of growth was observed for all samples. Simultaneously, the details of the crystalline structure are different for films that were grown on the different substrates. From the diffraction patterns of the films grown on the glass substrate, the single-phase nature of all films is clearly shown (Fig. 4). The lattice parameters of investigated films are presented in Table I. The first two films were deposited under the same conditions on glass and silicon substrates. It allows us to compare the behavior of thin-film solid solutions from the nature of the substrate.

The increase in the size of the lattice parameter in the samples with less thickness (set by less time of deposition) is probably related to the influence of the substrate during the formation of the nucleus. After increasing the film thickness, the lattice parameter remains unchanged within the accuracy of its determination.

Scanning electron microscopy (SEM) images of the surface of the Pb-Cd-Te film (with a magnification of 100 and 5000 times: Fig. 5(a) and (b), respectively) deposited on silicon substrate indicate the oriented growth caused by silicon. The location of the micro-cracks (Fig. 5a) corresponds to the

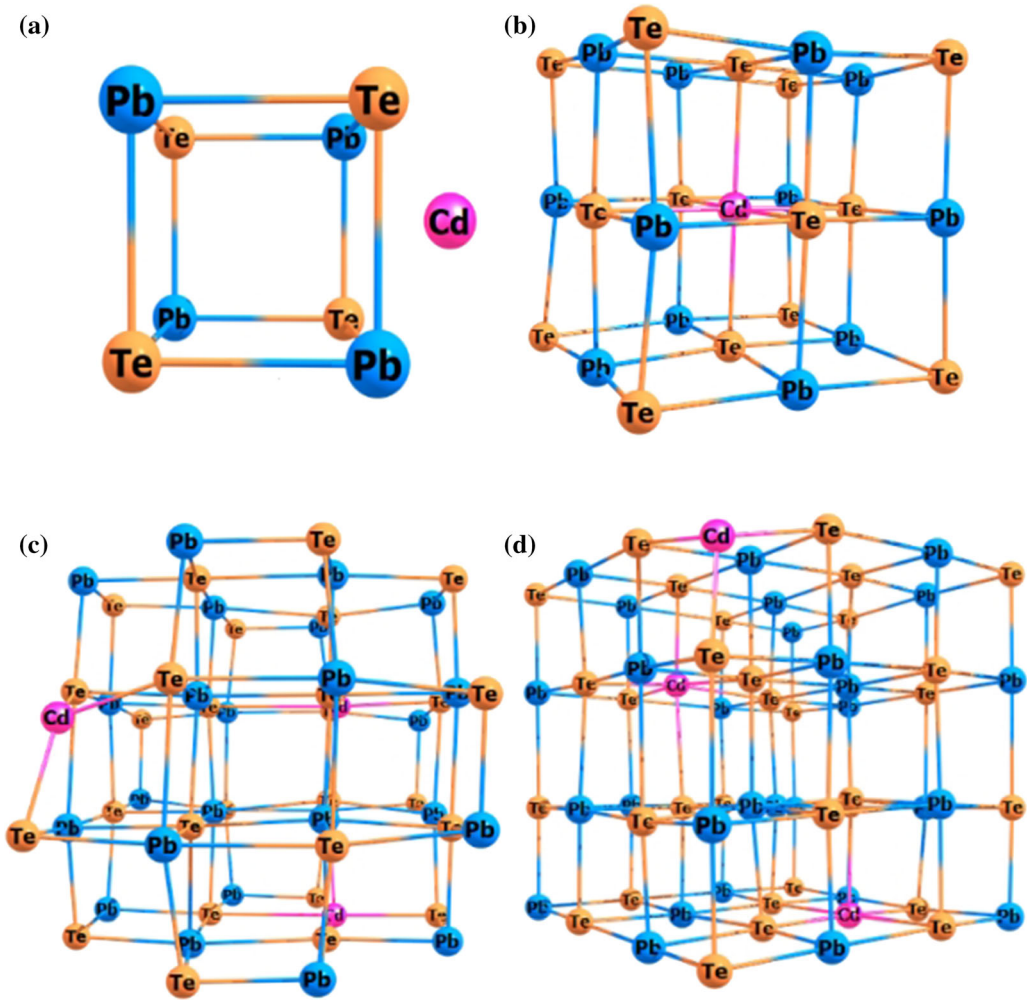

Fig. 1. The visualization of Pb-Cd-Te clusters: (a) Pb_4Te_4, (b) $Pb_{13}Cd_1Te_{13}$, (c) $Pb_{25}Cd_3Te_{28}$, and (d) $Pb_{29}Cd_3Te_{32}$.

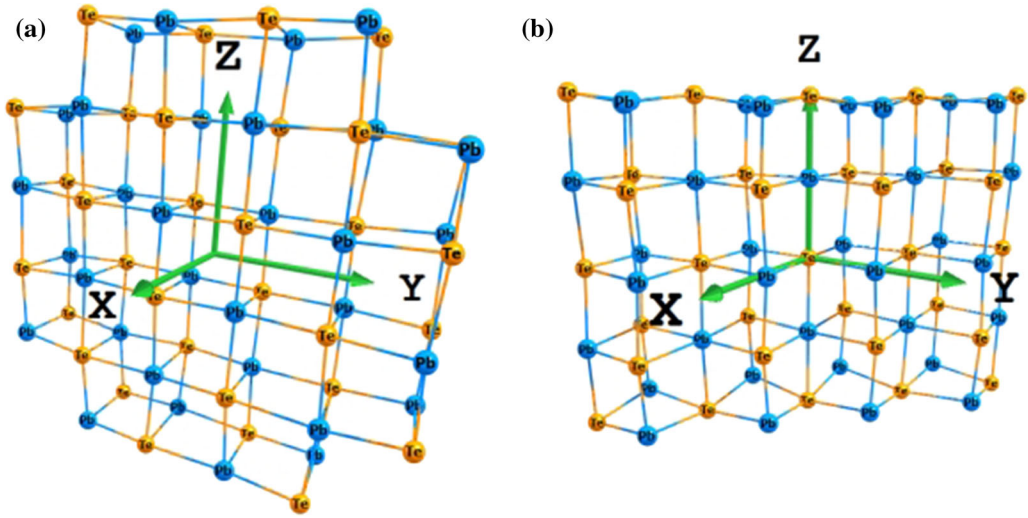

Fig. 2. The visualization of PbTe films with cleavage in the directions of (100) (a) and (110) (b).

structure of the substrate in the (100) direction. The magnification of the separate grain shows the uniform orientations of the nano-islands on the surface (Fig. 5b). The heights of the individual nano-islands are homogeneous.

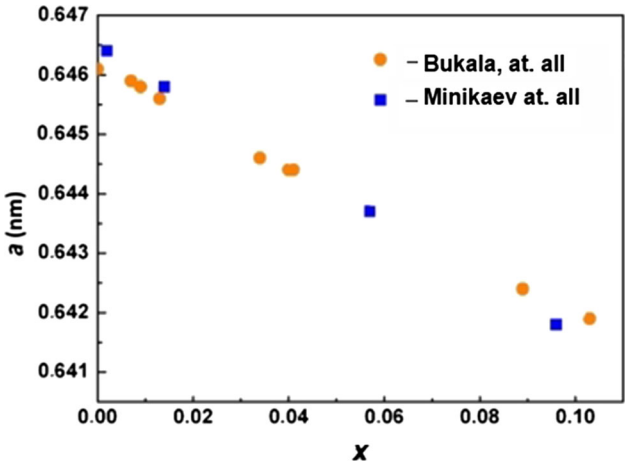

Fig. 3. The experimental lattice parameter as a function of x for $Pb_{1-x}Cd_xTe$ compounds: ●—,[9] ■—[10].

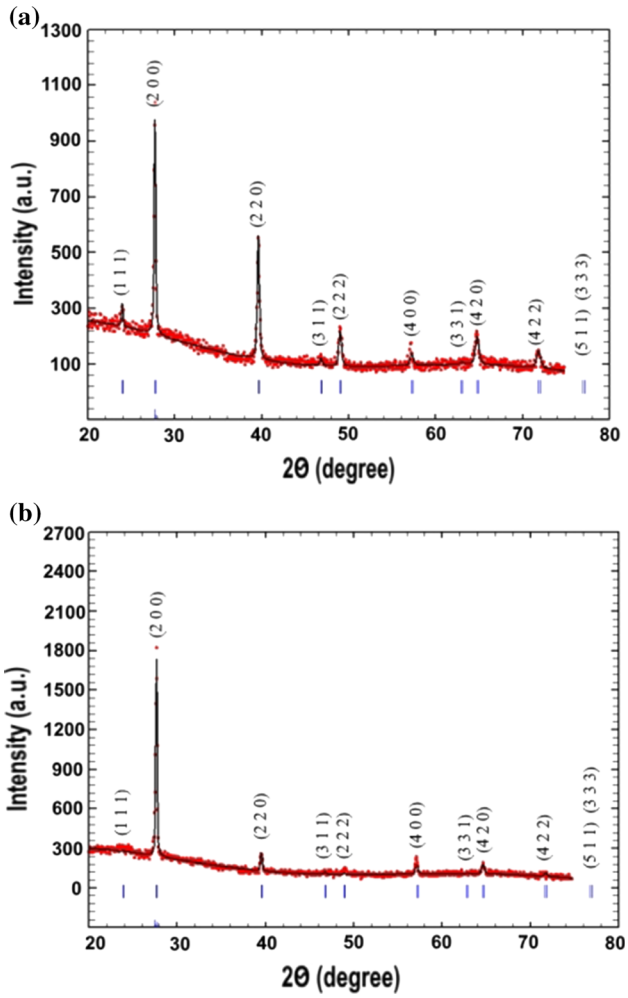

Fig. 4. X-ray diffraction patterns of $Pb_{0.9}Cd_{0.1}Te$:Pb (3 at.%) thin films deposited on glass substrates: (a) sample 1; (b) sample 2.

X-ray diffraction studies of $Pb_{0.9}Cd_{0.1}Te$: Pb (3 at.%) samples confirm these assumptions, as two more phases were detected: pristine Pb (~ 1.6 mass%) and impurities of CdTe (~ 3 mass%). Accordingly, the lattice parameter of such inclusions changes the value in the direction to increase: the main compound is characterized by a lattice parameter of 6.448 Å, and the inclusion of CdTe is about 6.481 Å. On the surface of the section of these phases, one can expect the changes in properties related to dimensional effects and charge redistribution due to the formation of new bonds. Such inclusions lead to stresses on the surface and in bulk.

The classical March–Dollase function is used for analysis of the powder diffraction patterns.[24] The degree of predominant orientation of crystallites was found as:

$$P_k = G_2 + (1 - G_2) \cdot W(\alpha), \tag{4}$$

where

$$W(\alpha) = \left(G_1^2 \cos^2 \alpha + \frac{\sin^2 \alpha}{G_1} \right)^{-3/2}. \tag{5}$$

Here, G_2 is the fraction of crystallites without predominant orientation, and $W(\alpha)$ is a weighting function for describing the proportion of crystallites in which the vectors h of the inverted lattice are parallel to the surface normal n of the sample. Considering that the powder method was used, the direction n is also the direction of the predominant orientation H. The angle α is the angle between the vectors h and H in the single crystal, that is, the acute angle between the scattering vector and the direction of the predominant orientation.

For films grown on glass substrates, the values of the parameter G_1 with increasing film thickness are 2.79 (216 nm in thickness) and 1.23 (297 nm in thickness), respectively. For the sample in which the surface is characterized by a set of flat plates, where the plate crystals are packed along the diffraction vector, the value of $G_1 < 1$, and in the case of needle crystals, the value of $G_1 > 1$. Accordingly, the crystallites on the surface of the film have an elongated shape along the direction perpendicular to the plane of growth. As the film thickness increases, the value of the parameter G_1 decreases to 0.1. The process of growth of such a film can be represented as follows. On the initial island surface, the growth after the deposition is accompanied by the growth of islands in the direction parallel to the surface of the substrate and filling the cavities to form plate crystallites. Thus, nucleus growth occurs by the Volmer–Weber mechanism,[41] which later transforms to form films by the Frank–van der Merwe mechanism. Such a change in growth mechanisms with deposition occurs for the following reasons. First, the formation of three-dimensional statistically located individual islands is observed through the efforts of the system to minimize the energy. Their base will be strongly deformed. The deformation decreases simultaneously with the

Table I. Measured values of lattice parameter *a* for $Pb_{0.9}Cd_{0.1}Te$:Pb (3 at.%) thin films deposited on glass and silicon substrates

Sample no.	Substrate materials Time of deposition, s	Glass		Silicon	
		Thickness, nm	*a*, Å	Thickness, nm	*a*, Å
1	80	338	6.436 ± 0.002	338	6.446 ± 0.001
2	60	297	6.432 ± 0.003	270	6.452 ± 0.001
3	20	216	6.446 ± 0.002		

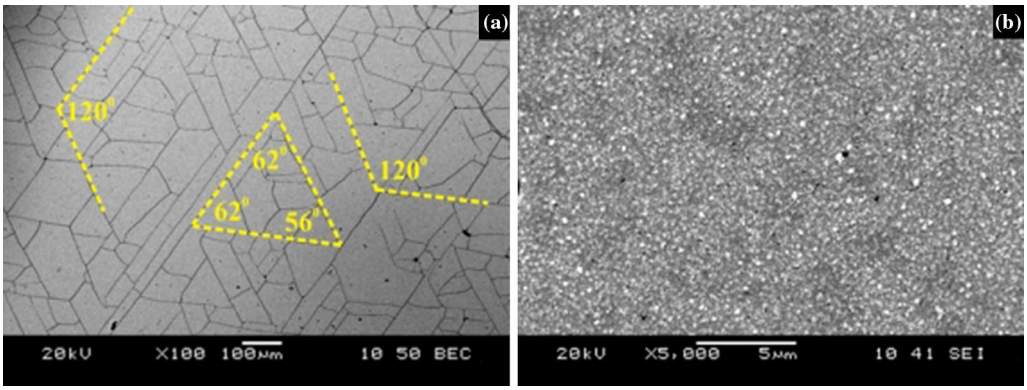

Fig. 5. SEM images for $Pb_{0.9}Cd_{0.1}Te$:Pb (3 at.%) thin films deposited on the silicon substrate with lower (a) and higher (b) magnification. The SEM image with lower magnification was obtained using the BEC-mode, and SEM image with the higher magnification was done using SEI-mode.

distance from the substrate to the vertices of the columnar structures. The growth of such nanostructures occurs until the stresses at the level of their vertices disappear entirely. Then, a sticking of these vertices is observed, which is reflected by the formation of lamellar structures on the film surface.

The growth plane of the films on silicon substrates is (100). This can be seen from the corresponding diffraction patterns (Fig. 6) by a single reflex (400) by Si. This conclusion is also confirmed by the SEM image in Fig. 5(a) (see above). The considerable intensity of the peak (100) of the film indicates the growth of the almost single-crystalline mosaic film. However, the presence of weak diffraction peaks of the film from other planes suggests that the film also has crystallites that grow in a disoriented manner. A deviation from the single-crystal form was observed when deposited on a glass substrate. The predominant orientation in the (200) direction is maintained, but the intensity of the other peaks increases because there is no one clear orientation of the substrate material. The deposition of polycrystalline material with different orientations of these crystallites on the amorphous glass substrate is natural. For example, in Ref. 42, the polycrystalline PbTe films on Si and glass substrates are obtained as a result of the epitaxial growth.

It was observed that a film of 338 nm in thickness has 95% of oriented crystals, and the film of 270 nm in thickness has 93% of such crystals. The value of

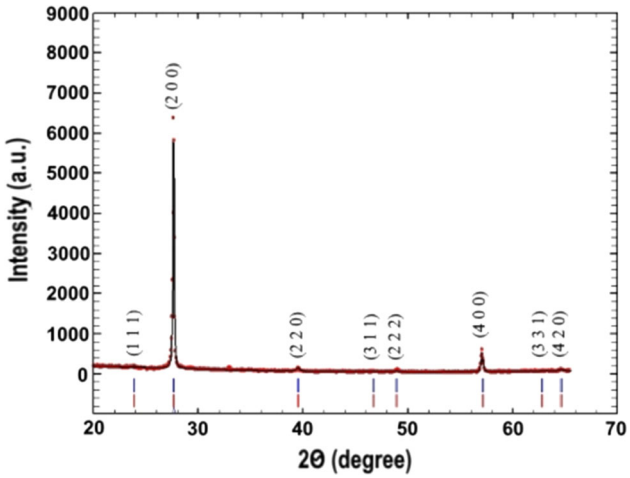

Fig. 6. The X-ray-diffraction pattern of $Pb_{0.9}Cd_{0.1}Te$:Pb (3 at.%) thin films deposited on silicon substrate (sample 1).

G_1 is equal to 14 and 18, respectively. Thus, such surface nanocrystals are needle-type. But, the ratio of their height to width decreases with increasing thickness, similar to the films grown on the glass substrate. Therefore, the growth of films on the silicon substrate is almost unidirectional, and a mechanism of growth is characterized by the Volmer–Weber mechanism. The lattice parameter of films decreases with increasing thickness. It is due to the decrease of the micro-stresses caused by

the significant difference between the lattice parameter of the film and the substrate. This mechanism of growth and the observed homogeneity of the composition of islands indicate that the rate of diffusion within the nano-islands is much greater than the rate of change of their radius (the rate of formation of surface nanotubes).[42]

The occurrence of cadmium atoms in the position of tellurium was simulated in accordance with the X-ray structural analysis (Fig. 7). During the calculation, the crystal lattice was distorted. The chalcogen atoms approached the introduced cadmium, and the metal atoms were moved away from it. The energetic advantage of replacing the Pb position by Cd is confirmed by the homogeneity of the structures studied with the X-ray data and SEM investigations. The evolution model of the specified substitution is shown in Fig. 7. Such transformations on the surface are energetically more likely. The possibility of such equilibrium positions at deeper levels in the bulk of material will require higher energy.

The simulation of the process of the cadmium atom replacement in solid solution was carried out for the $Pb_{32}Te_{32}$ cluster model.[43] The calculations of the Cd atom in each position of Pb with the formation of three-, four-, five-, and six-coordinated bonds were made separately. The formation energy of such a structure is the difference between the values of the total energy of the structure of the binary compound and a solid solution. The formation energy of the Cd_{Pb} defect at different positions in the surface structure with the formation of three-, four-, and five-coordinated bonds and inside the structure with the formation of six-coordinated bonds, equal to: δE_3 = 3.691 eV, δE_4 = 3.545 eV, δE_5 = 3.744 eV, and δE_6 = 3.844 eV, respectively.

The three-coordinated Cd atoms tend to form hexagonally arranged bonds (the angles between the bonds are about 106º) and to reduce the interatomic distance. The four- to five-coordinated Cd atoms also show a strong attraction to neighboring atoms. However, their symmetrical arrangements in the structure and the considerable degree of ionicity of the bonds in CdTe cause a smaller change in the interatomic distance and preserve the structure of the matrix of the primary compound. Cd atoms, which replace the Pb atoms, do not change the structure of the compound and form six bonds that cause charge irregularity in the vicinity of these defects.

The difference between the ionic radius between Cd (0.097 nm) and Pb (0.12 nm) can lead to the formation of quantum defects in the lattice.[6] Changing the distance between atoms in the new structure leads to change in the potential of the neighbor to the substituent cadmium and lead atoms, and is carried out to change of the binding energy of the surface electrons of chalcogen to their nuclei. Usually, the distances between Cd and Te in the ternary compound are higher, and therefore the electron binding energies for Cd atoms increase, and for Te, it decreases compared to binary compounds. Such redistribution leads to the local narrowing of the bandgap in the impurity atom region.

The types of bonding in the crystal structure and the density of electronic states (DOS) can be conveniently studied by analyzing the maps of the distribution of the spatial charge (Fig. 8). First, we can conclude that the Cd atom, which replaces the Pb atom, creates a local region of high charge gradient. The electron density around the chalcogen atoms is higher than around the metal atoms. The bonds are formed by the redistribution of charge between interacting atoms. Since the chalcogen contains six valence electrons and the Pb and Cd have four and two valence electrons, respectively, this situation is reasonable.

The surface plays a crucial role in the description of the properties of the system due to small size of the studied film structures. Namely, the contribution of DOS on the surface of films is about 84% of the contribution for the entire cluster (Fig. 9). Inclusions containing Cd also significantly affect the DOS in the bandgap and deep in the conductive band and valence bands (the value is ~ 31%).

Three- and five-coordinated Cd atoms independently form a noticeable accumulation of surface

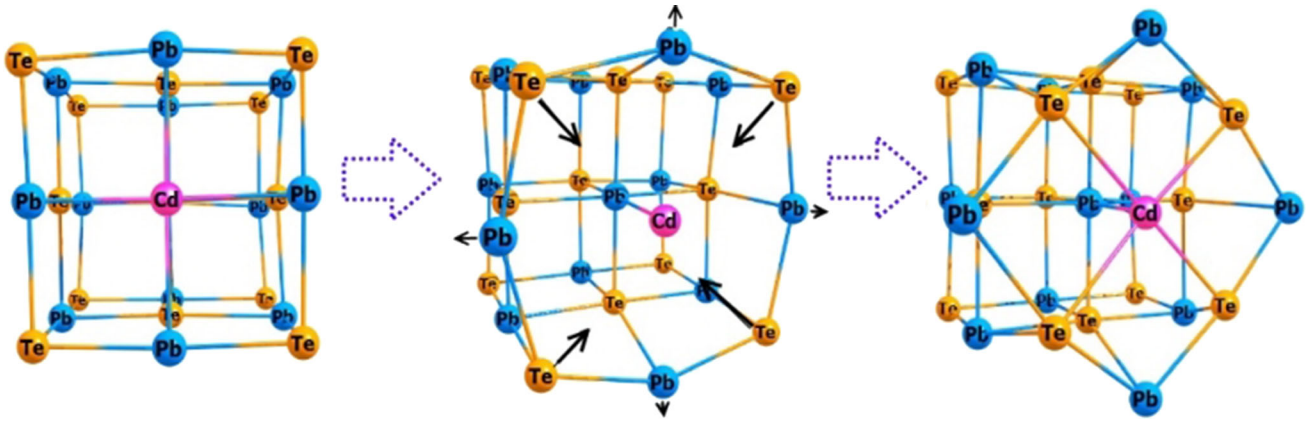

Fig. 7. The simulation of the Cd substitution of the anion position at the $Pb_{13}CdTe_{13}$ cluster surface.

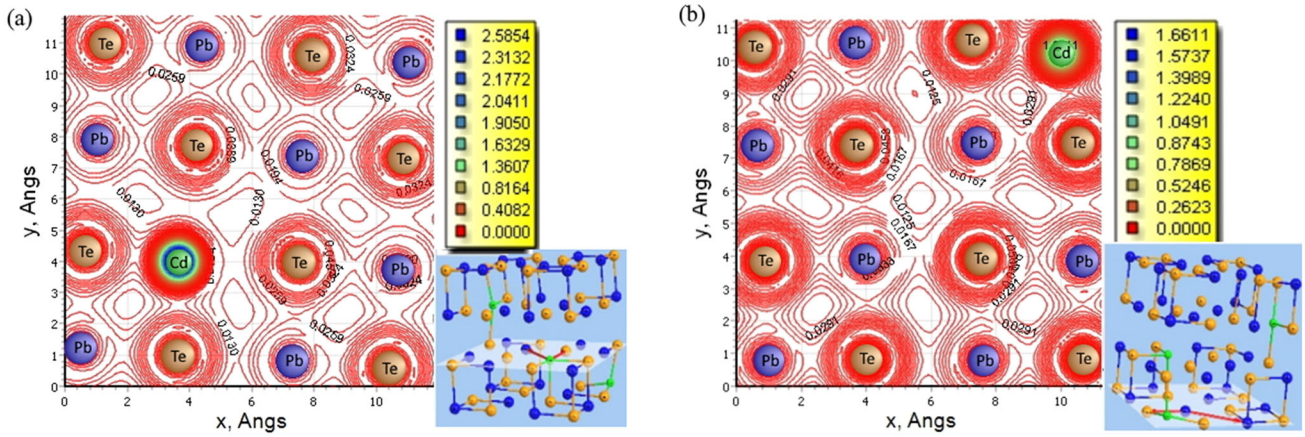

Fig. 8. Spatial charge distribution maps for $Pb_{13}CdTe_{13}$ cluster: (a) the Cd atom is located in the cluster, (b) Cd is located at the surface.

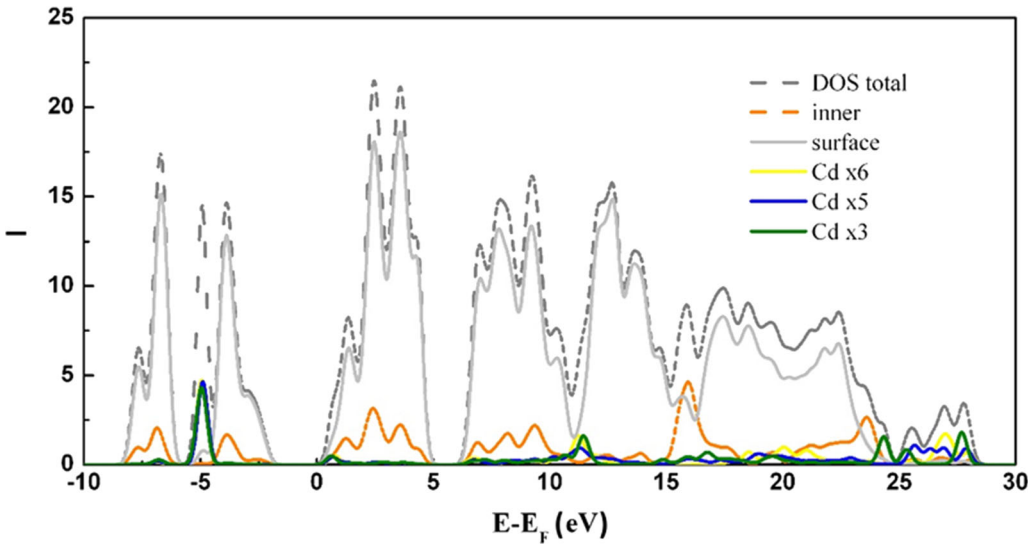

Fig. 9. The density of electronic states (DOS) for the $Pb_{29}Cd_3Te_{32}$ cluster: total DOS (dots), and the partial contributions of surface and internal atoms to the DOS.

charge. The impurity levels on the DOS (Fig. 9) are next: a significant peak in the valence band at −5 eV, and in the conductive band in the range 25–28 eV. The contribution of all three Cd atoms forms a small but noticeable peak near the Fermi level. It should be noted that due to such a significant influence on the DOS, the contributions of both atoms inside and on the surface differ little. It was indicated that the CdTe inclusions should significantly change the thermoelectric properties of materials based on the studied solid solutions.

The change of the thermodynamic properties of clusters was determined by increasing their size. The clusters were chosen taking into account the maxima of symmetry and composition of the structure. It should be noted that significant changes were observed only in small clusters (0.3–0.7 nm). The application of model approaches allows us to obtain a good match of the studied characteristics with the experimental data for structures containing ~ 60 atoms. Accordingly, it can be argued that clusters of such small sizes can be used for modeling of the materials.

The calculation of the equilibrium positions of atoms using the SBKJC-based functions allowed us to obtain the optimized coordinates of atoms in clusters. A rigid-molecule approximation[44,45] was used in our calculations. The clusters were represented by rigid blocks of which the crystal structure is composed. These values were used as initial values in the calculation of the fundamental oscillational, rotational, and translational frequencies. The methodology for calculating the thermodynamic parameters is based on the search for normal oscillation frequencies at which the determinant is zero. For these frequencies, the calculation of the statistical sum for the oscillatory components and the thermodynamic functions according to standard formulas has been performed. The formation energy ΔE, enthalpy of formation ΔH, entropy ΔS, Gibbs

energy ΔG, and heat capacity at constant volume of C_V were calculated, considering the sum of the components for each parameter: the electronic component, the vibrational component with an account of a zero-point parameter of vibrations, the rotational component, and the translational component.[46]

Changing the size of the cluster, and accordingly the number of atoms at the surface area, influences the values of the thermodynamic parameters (Fig. 10). Since the smallest cluster (Fig. 1a) contains only three-coordinated atoms, the graphs show much smaller values for the energy ΔE and enthalpy ΔH. Although, these values are close for all clusters since they are determined mainly by vibrational and rotational degrees of freedom. The opposite state is for Gibbs energy and entropy. Here, it is clear that both the behavior and the numerical values of these quantities with increasing the number of atoms in clusters differ significantly only for small clusters. The temperature dependence for Gibbs energy and entropy for 56 and 64 atoms coincides. The equations that describe the thermodynamic parameter tendencies versus temperature are shown in Table II.

The same situation was observed for the heat capacities at constant pressure C_P and volume C_V (Fig. 11). That is, we can conclude that the restriction of only cluster *d* (Fig. 1d), which includes 64 atoms, allows us to obtain both qualitatively and quantitatively reliable results. Thus, it is not necessary to perform computations for more complex clusters that require longer computations or significantly more expensive computer hardware.

The numerical values for the specific heat capacities in the entire studied temperature range are close for all clusters, but they do not exceed the values of the thermal heat capacities according to the Dulong–Petit law. The increase of clusters size, and thus reducing the ratio of surface area to bulk, is accompanied by a decrease in the fraction of the low-frequency vibrations of the phonon spectrum.

The number of broken bonds on the surface does not significantly affect the value of heat capacity. For $Pb_{25}Cd_3Te_{28}$ and $Pb_{29}Cd_3Te_{32}$ clusters, the number of atoms with the same coordination number is the same

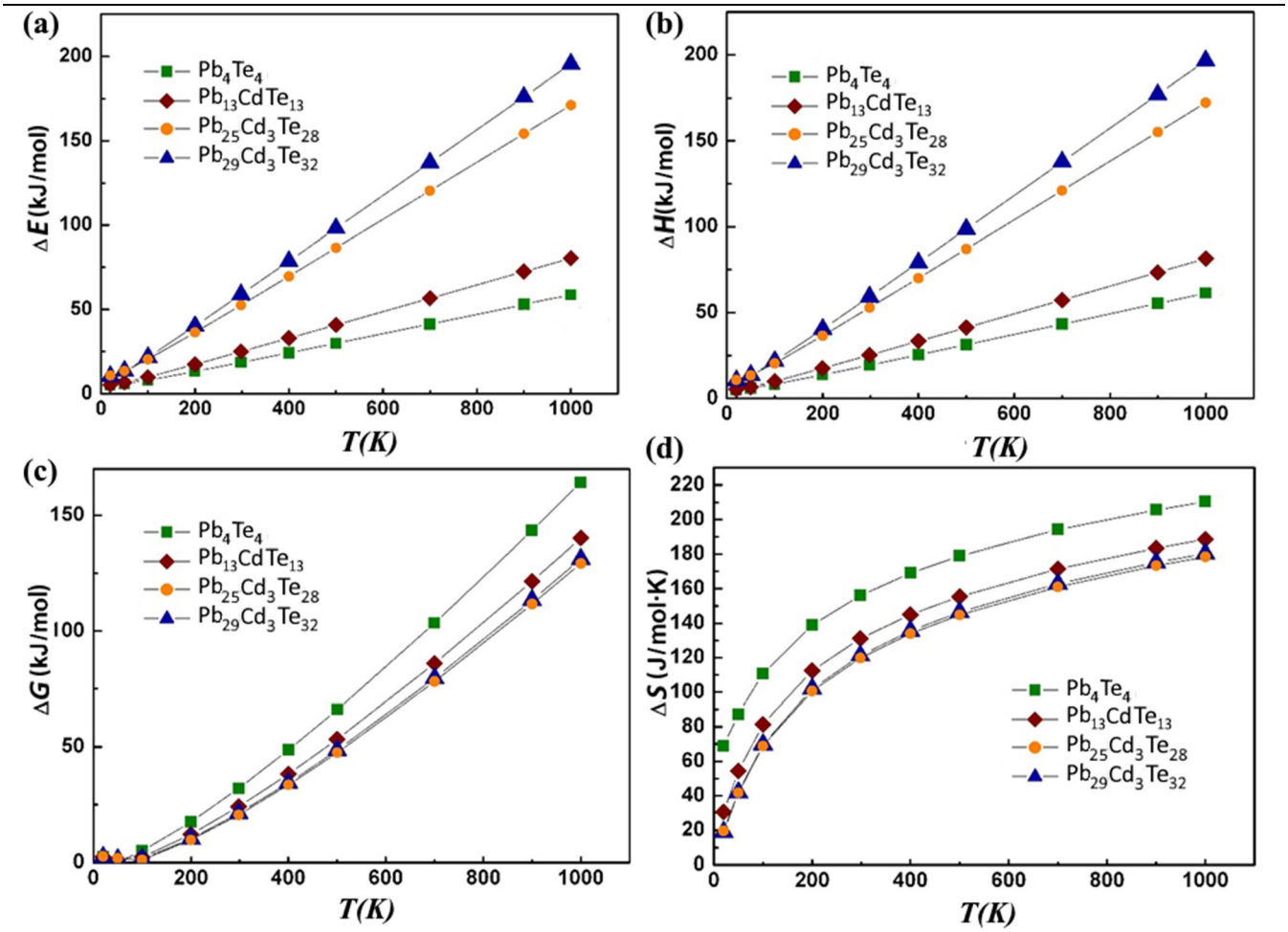

Fig. 10. The simulated formation energy ΔE (a), formation enthalpy ΔH (b), Gibbs free energy ΔG (c), and entropy ΔS (d) as a function of temperature for the investigated Pb-Cd-Te clusters.

Table II. Approximation coefficients (a_i, b_i, c_i) of temperature dependence of thermodynamic parameters $\Delta E(T)[\Delta H(T), \Delta G(T)] = a_i T + b_i$, $\Delta S(T) = a_i \ln(T) - b_i$, and $\Delta C_P(T) = a_i + b_i \cdot 10^{-3} \cdot T - c_i \cdot 10^5 \cdot T^{-2}$ at T = (50–1000) K

Thermodynamic parameter	Approximation coefficients			Number of atoms
	a_i, kJ/mol K	b_i, kJ/mol	c_i, kJ/mol K^2	
Energy of formation,	0.0776	2.3549		27
ΔE, kJ/mol	0.1658	4.4092		56
	0.1914	3.2373		64
Enthalpy,	0.0787	2.3549		27
ΔH, kJ/mol	0.1668	4.4092		56
	0.1926	3.2373		64
Entropy	41.873	104.83		27
ΔS, J/mol K	42.372	118.7		56
	43.022	121.13		64
Gibbs free energy,	0.0751	−3.0609		27
$-\Delta G$, kJ/mol	0.0607	−2.4522		56
	0.0644	−2.7844		64
Heat capacity,	43.4818	5.6229	0.109	27
C_P, J/mol K	44.2264	6.0759	0.1204	56
	45.0779	5.3517	0.1221	64

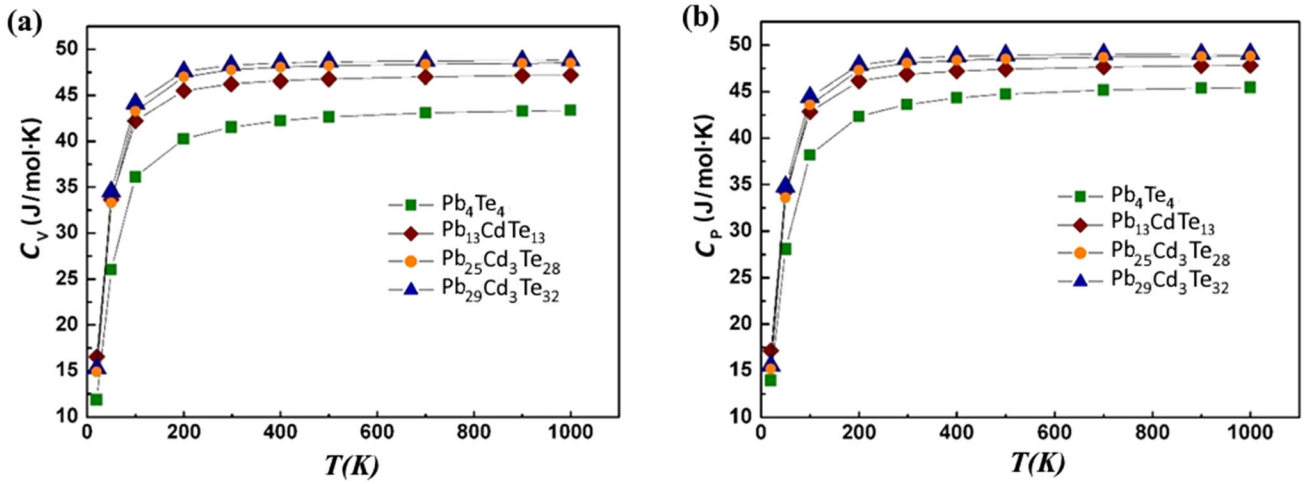

Fig. 11. The simulated specific capacities at constant volume C_V (a) and constant pressure C_P (b) as a function of temperature for the investigated Pb-Cd-Te clusters.

only for six-coordinated (internal) atoms, and the magnitude of the heat capacity of these clusters is almost indistinguishable. It can indicate that the numerical value of heat capacity is independent due to the number of degrees of freedom of the components of the system. The use of small clusters allows us to obtain satisfactory values of heat capacity (Table III) caused by compensation of the low-frequency cut-off phonon spectrum due to the finite size of them, and the excitation of low-frequency modes at low temperatures.

CONCLUSION

In this work, the open vacuum method was applied to obtain single-phase thin films with a high-quality surface, which is the main requirement for their successful practical applications. The structure of $Pb_{0.9}Cd_{0.1}Te$:Pb (3 at.%) films was rock salt in agreement with the DFT calculations.

Two types of substrates were used to identify the optimal technological conditions for film fabrication. It was found that Pb-Cd-Te films grown on the silicon substrate show higher preferred crystallographic orientation in comparison with the films deposited on the glass substrate. However, we also identify that the technological conditions can affect the crystallization of the films, and the use of the proper technological procedure makes it possible to fabricate films with fine distribution of crystalline blocks and without any impurity phases. The surface nanocrystals for $Pb_{0.9}Cd_{0.1}Te$:Pb (3 at.%) films on silicon substrate are needle-type. The crystallites on the surface of the film deposited on the glass substrate have an elongated shape along the

Table III. Thermodynamic parameters of cadmium telluride and lead telluride, and calculated values for solid solution $Pb_{0.9}Cd_{0.1}Te$: entropy (ΔS) and specific heat (C_P) at temperature 273.15 K

	CdTe	PbTe	$Pb_{0.9}Cd_{0.1}Te$
ΔS, J/mol K	100.4832[47] 100[48] 92.9[49]	110.0392 ± 0.2092[47] 110.04 ± 2.09[50]	121.2
C_p, J/mol K	50 ± 0.5[51,52]	50.554[53] 46.753[54]	48.5

direction perpendicular to the plane of growth. Aiming to find the proper position of Cd in the PbTe lattice, the defect formation energy calculations have been carried out. The introduction of the Cd atom into the Pb position was found to be the most energetically favorable scenario of defect formation.

The formation energy ΔE, formation enthalpy ΔH, entropy ΔS, Gibbs energy ΔG, and heat capacity have been calculated considering the rigid-molecule approximation and available crystallographic data. The numerical values for the specific heat capacity over the entire temperature range are similar for all clusters, however slightly lower in comparison with the Dulong–Petit limit. This finding is important for estimation of the thermal conductivity of the films. This work brings light on the fabrication process of the single-phase $Pb_{0.9}Cd_{0.1}Te$:Pb (3 at.%) thin films with a high-quality surface using the low-cost and simple method of open evaporation in a vacuum. Furthermore, such a method can be effectively applied for the other types of thermoelectric films.

ACKNOWLEDGMENTS

This study was supported by the Ministry of Education and Science of Ukraine as the joint Ukrainian-Belarus project “Synthesis, control and laser diagnostics of thermophysical properties of thin-film thermoelectric materials based on multicomponent compounds PbSnSeTe” and as the project for young scientists “Technology of thin-film thermoelectric micromodules based on multicomponent compounds with quantum-size effects”.

CONFLICT OF INTEREST

The authors declare that they have no conflict of interest.

REFERENCES

1. G. Tan, X. Zhang, S. Hao, H. Chi, T.P. Bailey, X. Su, C. Uher, V.P. Dravid, C. Wolverton, M.G. Kanatzidis, and A.C.S. Appl, *Mater. Interfaces* 11, 9197 (2019).
2. I.V. Horichok and T.O. Parashchuk, *J. Appl. Phys.* 127, 055704 (2020).
3. B. Dzundza, L. Nykyruy, T. Parashchuk, E. Ivakin, Y. Yavorsky, L. Chernyak, and Z. Dashevsky, *Physica B* 588, 412178 (2020).
4. Z. Dashevsky, *Lead Chalcogenides Physics and Application*, ed. D. Khokhlov (New York: Taylor & Francis, 2003).
5. E.A. Marquis, M. Hekmaty, A. Morales, and D.L. Medlin, *Microsc. Microanal.* 13, 1646 (2007). https://doi.org/10.1017/S1431927607075496.
6. S. Kumar, Z.H. Khan, M.M. Khan, and M. Husain, *Curr. Appl. Phys.* 5, 561 (2005).
7. L. Nykyruy, M. Ruvinskiy, E. Ivakin, O. Kostyuk, I. Horichok, I. Kisialiou, Y. Yavorskyy, and A. Hrubyak, *Physica E* 106, 10 (2019).
8. T. Parashchuk, O. Kostyuk, L. Nykyruy, and Z. Dashevsky, *Mater. Chem. Phys.* 253, 123427 (2020).
9. M. Bukała, P. Sankowski, R. Buczko, and P. Kacman, *Phys. Rev. B: Condens. Matter* 86, 085205 (2012).
10. R. Minikayev, E. Dynowska, P. Dziawa, E. Kamińska, and A. Szczerbakow, in *VIII KSUPS 2009: Extended Abstracts/Synchrotron Radiation in Natural Science*, vol. 8, p. 83 (2009).
11. S. Lalitha, S.Z. Karazhanov, P. Ravindran, S. Senthilarasu, R. Sathyamoorthy, and J. Janabergenov, *Physica B* 387, 227 (2007).
12. R. Dalven, *Infrared Phys.* 9, 141 (1969).
13. X. Wang, I. Veremchuk, M. Bobnar, J.-T. Zhao, and Y. Grin, *Inorg. Chem. Front.* 3, 1152 (2016).
14. M. Lingg, A. Spescha, S.G. Haass, R. Carron, S. Buecheler, and A.N. Tiwari, *Sci. Technol. Adv. Mater.* 19, 683 (2018).
15. D. Wu, L.-D. Zhao, F. Zheng, L. Jin, M.G. Kanatzidis, and J. He, *Adv. Mater.* 28, 2737 (2016).
16. R. Rustom-Dalouche, S. Rolland, R. Granger, and C.M. Pelletie, *Phys. Status Solidi B* 129, 835 (1985).
17. H. Ibach, *Physics of Surfaces and Interfaces*, Vol. 12 (Berlin: Springer, 2006).
18. W. Mönch, *Semiconductor Surfaces and Interfaces* (Berlin: Springer, 2001), pp. 81–103.
19. H. Wu, J. Si, Y. Yan, Q. Liao, and Y. Lu, *Appl. Surf. Sci.* 356, 742 (2015).
20. R. Vengrenovich, B. Ivanskii, I. Panko, and M. Stasyk, *J. Phys. Chem. C* 117, 13681 (2013).
21. H.J. You, H.S. Chu, W.J. Li, and W.L. Lee, *J. Power Sources* 438, 227055 (2019).
22. A. Dauscher, M. Dinescu, O.M. Boffoué, A. Jacquot, and B. Lenoir, *Thin Solid Films* 497, 170 (2006).
23. M.A. Herman, W. Richter, and H. Sitter, *Epitaxy: Physical Principles and Technical Implementation*, Vol. 62 (Berlin: Springer, 2013).
24. I. Yaremiy, S. Yaremiy, V. Fedoriv, O. Vlasii, and A. Lucas, *Eastern-Eur. J. Enterp. Technol.* 5, 61 (2018).
25. C. Lee, W. Yang, and R.G. Parr, *Phys. Rev. B* 37, 785 (1988).
26. M.W. Schmidt, K.K. Baldridge, J.A. Boatz, S.T. Elbert, M.S. Gordon, J.H. Jensen, S. Koseki, N. Matsunaga, K.A. Nguyen, S.J. Su, T.L. Windus, M. Dupuis, and J.A. Montgomery, *J. Comput. Chem.* 14, 1347 (1993).
27. M.S. Gordon and M.W. Schmidt, Chapter 41.*Theory and Applications of Computational Chemistry, the First Forty Years*, ed. C.E. Dykstra, G. Frenking, K.S. Kim, and G.E. Scuseria (Amsterdam: Elsevier, 2005), pp. 1167–1189.
28. A.D. Becke, *J. Chem. Phys.* 98, 5648 (1993).
29. K. Hummer, A. Grüneis, and G. Kresse, *Phys. Rev. B: Condens. Matter* 75, 195211 (2007).
30. A.J. Miller, G.A. Saunders, and Y.K. Yogurtcu, *J. Phys. C: Solid State Phys.* 14, 1569 (1981).

31. J. An, A. Subedi, and D.J. Singh, *Solid State Commun.* 148, 417 (2008).
32. D. Freik, T. Parashchuk, and B. Volochanska, *J. Cryst. Growth* 402, 90 (2014).
33. R. Ahiska, D. Freik, T. Parashchuk, and I. Gorichok, *Turk. J. Phys.* 38, 125 (2014).
34. L.I. Nykyruy, T.O. Parashchuk, and B.P. Volochanska, *Chalcogenide Lett.* 13, 239 (2016).
35. S. Ahmad, S.D. Mahanti, K. Hoang, and M.G. Kanatzidis, *Phys. Rev. B: Condens. Matter* 74, 155205 (2006).
36. L.I. Nykyruy, B.P. Naidych, O.M. Voznyak, T.O. Parashchuk, and R.V. Ilnytskyi, *Semicond. Phys. Quant. Electron. Optoelectron.* 22, 156 (2019).
37. E. Saucedo, L. Fornaro, V. Corregidor, and E. Diéguez, *Eur. Phys. J.-Appl. Phys.* 27, 427 (2004).
38. B.A. Orlowski, A. Szczerbakow, P. Dziawa, K. Gas, A. Reszka, B.J. Kowalski, S. Thiess, and W. Drube, *Nucl. Instrum. Methods Phys. Res. Sect. B* 364, 132 (2015).
39. V.L. Deringer and R. Dronskowski, *J. Phys. Chem. C* 117, 24455 (2013).
40. M.A. Barote, A.A. Yadav, and E.U. Masumdar, *J. Chem. Biol. Phys. Sci.* 3, 510 (2013).
41. J.A. Venables and G.D.T. Spiller, *Surface Mobilities on Solid Materials* (Boston, MA: Springer, 1983), pp. 341–404.
42. A.V. Osipov, *Phys. Met.* 13, 26 (1991).
43. B.P. Naidych and O.B. Kostyuk, *Phys. Chem. Solid State* 21, 254 (2020).
44. D.C. Young, *Computational Chemistry: A Practical Guide for Applying Techniques to Real-World Problems* (New York: John Wiley & Sons Inc, 2001).
45. W.M. Haynes, *CRC Handbook of Chemistry and Physics : A Ready-Reference Book of Chemical and Physical Data* (Boca Raton, FL: CRC Press, 2010).
46. I.V. Horichok, L.I. Nykyruy, T.O. Parashchuk, S.D. Bardashevska, and M.A. Pylyponuk, *Mod. Phys. Lett. B* 30, 1650172 (2016).
47. N.Kh. Abrikosov, V.F. Bankina, L.V. Poretskaya, L.E. Shelimova, and E.V. Skudnova, *Semiconducting in II–VI, IV–VI, and V–VI Compounds* (New York: Springer, 1969).
48. J.A. Dean, *Lange's Handbook of Chemistry* (New York: McGraw-Hill Professional, 1999).
49. L. Mu, Ch Feng, and H. He, *MATCH Commun. Math. Comput. Chem.* 57, 111 (2007).
50. E. Guneri, F. Gode, and S. Cevik, *Thin Solid Films* 589, 578 (2015).
51. K. Yamaguchi, K. Hongo, K. Hack, I. Hurtado, and D. Neuschutz, *Mater. Trans. JIM* 41, 790 (2000).
52. P. Goldfinger and M. Jeunehomme, *Trans. Faraday Soc.* 59, 2851 (1963).
53. R.A. Robie, B.S. Hemingway, and J.R. Fisher, *Thermodynamic Properties of Minerals and Related Substances at 298,15 K and 1 Bar (105 Pascals) Pressure and at Higher Temperatures* (Washington: 1978).
54. Y. Bencherif, A. Boukra, A. Zaoui, and M. Ferhat, *Infrared Phys. Technol.* 54, 39 (2011).